Presented at the 2000 Western States Spring Meeting/The Combustion Institute, March 13-14, Paper number WS 00S-11

NUMERICAL STUDY OF BUOYANCY EFFECTS ON TRIPLE FLAMES

J.-Y. Chen

6163 Etcheverry Hall
University of California at Berkeley,
Berkeley, CA 94720,

T. Echekki

Combustion Research Facility, Sandia National Labs.
Livermore, CA 94550

ABSTRACT

The structure and propagation properties of triple flames subject to buoyancy effects are studied numerically using a high accuracy scheme. A wide range of gravity conditions, heat release, and mixing widths for a scalar mixing layer are computed for 'upright' and 'inverted' triple flames (i.e, gravity pointed in parallel and in opposite directions of flame propagation). These results are used to identify non-dimensional quantities, which parameterize the triple flame response. Computed results show that buoyancy effects act primarily to modify the overall size of the triple flame in response to gas acceleration through the two premixed branches. The impact of buoyancy on the structure of triple flame is found less pronounced than the general physical shape of the branches. The trailing diffusion branch is affected by buoyancy primarily due to the changes in the overall flame shape. The overall size of triple flame is determined by the two premixed branches. Buoyancy affects the locations of these premixed flames and consequently modifies the rates of diffusion of excess fuel and oxidizer from the premixed branches to the diffusion branch. A simple analytical model for the triple flame, which accounts for both buoyancy and heat release is developed. Comparisons of the proposed model for the triple flame speed with the numerical results for a wide range of gravity, heat release and mixing width conditions, yield good agreement.

INTRODUCTION

Since the work of Phillips (1965) more than three decades ago, there has been a growing interest in the study of triple flames (Buckmaster and Matalon, 1988; Hartley and Dold, 1991; Chung and Lee, 1991; Kioni, et al, 1993; Lee et al, 1994; Ruetsch, et al 1995; Domingo and Vervisch, 1996; Vedarjan and Buckmaster, 1998; Plessing et al, 1998; Daou and Linan, 1998; Echekki and Chen, 1998). The interest is largely motivated by the potential roles these structures may play in the burning of partially-premixed mixtures. This role is critical for both the stabilization and ignition in diffusion flames (e.g., Phillips, 1965; Chung and Lee, 1991).

Heat release is known to play an important role in the enhancement of the triple flame propagation speed as demonstrated by the numerical studies of Ruetsch et al (1995). Recently, Echekki and Chen (1998) and Im and Chen (1999) explored the coupling of heat release with preferential and differential diffusion effects and chemistry. Their studies show that to first order, the enhancement of the triple flame speed is primarily attributed to the heat release. The contribution of differential and preferential diffusions to the triple flame speed especially near the leading edge (the triple point) of the triple flame is within 10 % or less. However, in the triple point region, the flame structure is strongly modified by the combined leading edge curvature and the diffusion of H_2 and the H radical. These studies also show, as proposed by Ruetsch et al (1995), that the triple flame propagation speed may be approximated to first order by the square-root of the density ratio across the triple flame. This simple correlation is valid for the range of moderate scalar mixing layer thickness as evidenced by the mixture fraction gradient. Recent analysis and computations by Daou and Linan (1998) show that under strain and non-unity Lewis number conditions significant departure of the triple flame speed from the laminar planar value may be achieved even in the absence of heat release. The physical mechanism that contributes to the enhancement of the triple flame speed with heat release is associated with streamlines' divergence ahead of the premixed branches followed by their subsequent convergence farther downstream.

Because of the role played by flow around the flame in the enhancement of the triple flame speed, the coupling between heat release and gravity is also expected to be important. In this study we attempt to elucidate the nature of this coupling by computational studies of the structure and propagation of triple flames in a scalar mixing layer. An additional objective of this study is to understand the effects of gravity on the flame structure. Because of the effects of gravity on streamline divergence ahead of the flame, the width of the triple flame branches may be affected by gravity. As a result, the diffusion fluxes to the diffusion flame branch may be altered to affect its structure. We will first consider a diffusionally-neutral mixture (the effective Lewis numbers of both the fuel and oxidizer sides are equal to unity). We also consider a simple finite-rate kinetic model with heat release. No mechanisms for heat loss or confinement are imposed on the triple flames. Only triple flame configurations where the gravity vector is aligned with the triple flame axis (direction of flame propagation) are considered in this study. A parametric study is then carried out where the magnitude and sign of the gravity vector is varied to simulate a relatively wide range of conditions of gravity for downward-

propagating (the sign of gravity vector is in the same direction as the triple flame propagation) and upward-propagating triple flames.

The objective of this work is to study the effects of the buoyancy on the structure and propagation of triple flames configuration by a series of numerical simulations of triple flames in a simple scalar mixing. First, the governing equations and numerical implementation of the solution of the triple flames are presented. Second, discussions of the computed effects of buoyancy on triple flame structure and propagation are given. Third, results of a series of parametric runs are presented to explore the relationship between the triple flame propagation speed and the buoyancy. A simple model of the dependence of the triple flame speed on the buoyancy and heat release is proposed. The model is compared to the computed triple flame speeds over a wide range of parameters. Finally, a summary of the results is presented.

GOVERNING EQUATIONS

A two-dimensional computational domain is used for modeling the triple flames. The stream-wise coordinate will be denoted by *x* and the transverse coordinate by *y*. Summarized below are the governing equations.

Continuity:

$$\frac{\partial \rho}{\partial t}+\frac{\partial \rho u}{\partial x}+\frac{\partial \rho v}{\partial y}=0, \tag{1}$$

where *u* and *v* are the stream-wise velocity and transverse velocity respectively.

Momemtum equation in the stream-wise direction:

$$\frac{\partial \rho u}{\partial t}+\frac{\partial (\rho u^2+P)}{\partial x}+\frac{\partial \rho uv}{\partial y}=\frac{\partial \tau_{xx}}{\partial x}+\frac{\partial \tau_{xy}}{\partial y}+\rho \,|\,\vec{g}\,|\cos\phi, \tag{2}$$

where ϕ is the angle between the gravity vector and the unit vector in the stream-wise direction and $\vec{g}$ is the gravity force. The stresses τ_{xx} and τ_{xy} are given by

$$\tau_{xx}=\mu\left(2\frac{\partial u}{\partial x}-\frac{2}{3}(\frac{\partial u}{\partial x}+\frac{\partial v}{\partial y})\right), \tag{3}$$

$$\tau_{xy}=\mu\left(\frac{\partial u}{\partial y}+\frac{\partial v}{\partial x}\right), \tag{4}$$

where μ is the visocity with a temperature dependence as

$$\mu=\mu_0\left(\frac{T}{T_0}\right)^a \tag{5}$$

with a=0.76. The reference state, denoted by the subscript 0, is taken in the incoming flow which is assumed to have a uniform temperature. Similarly, the conservation equation of momentum in the cross-stream direction:

$$\frac{\partial \rho v}{\partial t}+\frac{\partial \rho u v}{\partial x}+\frac{\partial(\rho v^2+P)}{\partial y}=\frac{\partial \tau_{yx}}{\partial x}+\frac{\partial \tau_{yy}}{\partial y}+\rho\,|\,\vec{g}\,|\sin\phi\,. \tag{6}$$

The stresses τ_{yy} and τ_{yx} are given by

$$\tau_{yy}=\mu\left(2\frac{\partial v}{\partial y}-\frac{2}{3}(\frac{\partial u}{\partial x}+\frac{\partial v}{\partial y})\right), \tag{7}$$

$$\tau_{yx}=\tau_{xy}\,. \tag{8}$$

Assuming the ideal gas law, P=ρRT, the equation for total energy, $\rho E=\frac{\rho}{2}\left(u^2+v^2\right)+\frac{P}{\gamma-1}$, is

$$\begin{aligned}\frac{\partial \rho E}{\partial t}+\frac{\partial(\rho E+P)u}{\partial x}+\frac{\partial(\rho E+P)v}{\partial y}&=\frac{\partial}{\partial x}\left(u\tau_{xx}+v\tau_{yx}\right)+\frac{\partial}{\partial y}\left(u\tau_{xy}+v\tau_{yy}\right)\\&-\frac{\partial q_x}{\partial x}-\frac{\partial q_y}{\partial y}-Q_F\dot{w}_f+\rho\,|\,\vec{g}\,|\,(u\cos\phi+v\sin\phi),\end{aligned} \tag{9}$$

where γ is the ratio of species heats, c_p/c_v, assuming to be a constant value of 1.4. Q_F is the heat of reaction per unit mass of fuel burned, $\dot{w}_F$ is the fuel consumption rate by chemical reaction, and q_x and q_y are heat fluxes given by

$$q_x=-\lambda\frac{\partial T}{\partial x}\quad\text{and}\quad q_y=-\lambda\frac{\partial T}{\partial y} \tag{10}$$

with λ being the thermal conductivity. The combustion process is described by the equations for the fuel and oxidizer mass fractions, Y_F and Y_O as

$$\frac{\partial \rho Y_F}{\partial t}+\frac{\partial \rho u Y_F}{\partial x}+\frac{\partial \rho v Y_F}{\partial y}=\frac{\partial}{\partial x}\left(\rho D_F\frac{\partial Y_F}{\partial x}\right)+\frac{\partial}{\partial y}\left(\rho D_F\frac{\partial Y_F}{\partial y}\right)+\dot{w}_F \tag{11}$$

and

$$\frac{\partial \rho Y_O}{\partial t}+\frac{\partial \rho u Y_O}{\partial x}+\frac{\partial \rho v Y_O}{\partial y}=\frac{\partial}{\partial x}\left(\rho D_O\frac{\partial Y_O}{\partial x}\right)+\frac{\partial}{\partial y}\left(\rho D_O\frac{\partial Y_O}{\partial y}\right)+\dot{w}_O \tag{12}$$

with D_F and D_O being the mass diffusivities of fuel and oxidizer respectively. The thermal conductivity and mass diffusivities are temperature dependent and their values are determined by assuming constant values of Lewis and Prandtl numbers as

$$Le_F = \frac{\lambda}{\rho c_p D_F}, \qquad Le_O = \frac{\lambda}{\rho c_p D_O}, \qquad \mathrm{Pr} = \frac{\mu c_p}{\lambda}. \tag{13}$$

In the study, we set Le_F=Le_O=1 and Pr=0.75. The combustion process is modeled by a one-step chemical reaction as

$$\mathrm{F} + \mathrm{O} \rightarrow \mathrm{P}, \tag{14}$$

where the stoichiometric coefficients are unitary for simplicity. The reaction rate has the following Arrhenius form

$$\dot{w} = A\rho^2 Y_F Y_O \exp\left(-\frac{T_a}{T}\right), \tag{15}$$

where T_a is the activation temperature and A is the pre-exponential factor. With the non-dimensional temperature (θ), the heat release parameter (α), the Zeldovich number (β), and the reduced pre-exponential factor (Λ),the above reaction rate can be expressed as

$$\dot{w} = \Lambda\rho Y_F \rho Y_O \exp\left(-\frac{\beta(1-\theta)}{1-\alpha(1-\theta)}\right), \tag{16}$$

where $\theta = (T - T_0)/(T_\infty - T_0)$, $\alpha = (T_\infty - T_0)/T_\infty$, $\beta = \alpha T_a / T_\infty$, and $\Lambda = A\exp(-\beta/\alpha)$ with T_0 being the inlet temperature and T_∞ the adiabatic flame temperature of the stoichiometric mixture. The molecular weights of fuel and oxidizer are assumed to be equal and the consumption rates of fuel and oxidizer can be expressed as $\dot{w}_F = \dot{w}_O = -\dot{w}$.

NUMERICAL METHOD AND RUNNING CONDITIONS

The compressible Navier-Stokes equations along with the conservation equations for reactants are solved in a two-dimensional domain. Spatial derivatives are approximated by a sixth-order compact difference algorithm and the equations are integrated in time with a third-order Runge-Kutta scheme. Boundary conditions are specified using the Navier-Stokes characteristic boundary conditions (Poinsot and Lele, 1992). At the inlet of the computational domain, a uniform inflow velocity profile is prescribed and the mass fraction distributions of fuel and oxidizer are specified by

$$Y_F = \frac{1}{2}\left[1 - erf\left(\frac{y}{W}\right)\right] \quad \text{and} \quad Y_O = \frac{1}{2}\left[1 + erf\left(\frac{y}{W}\right)\right], \tag{17}$$

where erf is the error function, W is the characteristic mixing width, and y is assigned to be zero at the middle of the computational domain such that the plane with y=0 corresponds to the stoichiometric mixture. An outflow boundary condition is specified at the outlet of computational domain and non-reflective boundary conditions are imposed

on all sides. The buoyancy is described by the Froude number based on the planar premixed flame speed and a characteristic length scale. Two possible choices are considered: the width of the incoming mixing layer and the thickness of the stoichiometric planar premixed flame. In order to take into account the orientation of gravity force relative to the incoming flow, we define the following Froude number based on the width of mixing layer at the inlet as

$$\begin{aligned} Fr_w &= \frac{S_L^{\,2}}{|\vec{g}|W} \qquad \text{if sign}\{\cos(\phi)\} \le 0 \\ &= -\frac{S_L^{\,2}}{|\vec{g}|W} \qquad \text{otherwise,} \end{aligned} \tag{18}$$

where *sign{x}* is the sign of variable *x*. Similarly, we replace *W* by the thickness of planar stoichiometric premixed flame, L_f, we will have another Froude number as

$$Fr_{L_f} = Fr_w \frac{L_f}{W}. \tag{19}$$

Positive values correspond to triple flames propagating into the direction where gravity force is pointed and vice versa. Table 1 lists the conditions and the range of parameters explored in this study. The numerical simulations were carried out with a uniform grid system of 121x241 grids (stream-wise direction x transverse direction) with a physical region of about 40x80 flame thickness. Exploration runs with twice of grid points have been conducted showing differences within 1% in terms of deduced flame propagation speed. The steady-state solution of the triple flame structure is obtained using a similar numerical technique described by Ruetsch, et al., 1995. Steady state solutions without gravity force were obtained first and they were used as initial conditions for subsequent runs with buoyancy effects to save time. The typical CPU time for one run on a Pentium II 450 Mz machine running on Linux takes about 72 hours.

RESULTS AND DISCUSSIONS

General Features of Triple Flames

The general characteristics of a triple flame are briefly described here to provide the necessary background for the discussions of the effects of buoyancy on triple flames. Figure 1 presents the computed contours of axial velocity and fuel consumption rate in a two-dimensional domain. The fluids enter the domain at the left side of the boundary moving toward to the right. A mixing layer of fuel and oxidizer is prescribed at the inlet boundary. As seen in the reaction rate contour, the triple flame is featured by the three branches of the most intensively burning zone. The two "wings" correspond to the two premixed flames, one being rich and the other one being lean. The "tail" behind the two wings denote the location of a stochiometric nonpremixed flame. Unburned fuel and oxidizer behind the two premixed flames diffuse toward each other and burn rigorously at the stoichiometric location. As the triple propagates upstream, the fluids ahead of the triple flame tip is slowed down causing the streamline to diverge. As a result of intense heat release at the triple flame, the fluids accelerate significantly across the triple flame

tip. Downstream of the triple flame tip, the fluids gradually decelerate as the hot gas behind the flame tip expands.

The propagation speed of the triple flame is computed by tracking an interface corresponding to a fixed fuel mass fraction and evaluating its displacement speed (Echekki and Chen, 1998). This displacement speed, S_D, is evaluated within or near the reaction zone and it is expressed by

$$S_D = \frac{\frac{\partial}{\partial x}\left(\rho D_F \frac{\partial Y_F}{\partial x}\right) + \frac{\partial}{\partial y}\left(\rho D_F \frac{\partial Y_F}{\partial y}\right) + \dot{\omega}_F}{\rho\sqrt{\frac{\partial Y_F}{\partial x}\frac{\partial Y_F}{\partial x} + \frac{\partial Y_F}{\partial y}\frac{\partial Y_F}{\partial y}}}. \tag{20}$$

However, this speed measures the local displacement of the iso-scalar relative to the gas mixture locally. In the current coordinates, the propagation direction is opposite of the stream-wise direction. To evaluate the triple flame propagation speed, the total speed of the iso-scalar contour at the triple flame tip (gas velocity plus displacement speed), is subtracted from the cold gas velocity far upstream of the triple flame as

$$S_p = -\{[u + (-S_D)] - u_0\} = (S_D - u) + u_0, \tag{21}$$

where u is the magnitude of gas velocity in the stream-wise direction, u_0 is the magnitude of unburned gas velocity at the inlet of the computational domain. Note that Previous analytic and numerical studies (e.g., Hartley and Dold, 1991; Ruetsch, et al., 1995; Ghosal and Vervisch, 2000) showed that the propagating speed decreases with increasing mixture fraction gradient due to the effects of flame curvature, but increases with heat release due to the divergence effects of flow field.

Effects of Buoyancy

The above results serve as a base line for comparison with triple flames under the influence of buoyancy. The computed global effects of buoyancy on triple flames are exemplified in Figure 2 with $1/Fr_w$=-1 (ϕ=180^o), 0, and 1 (ϕ=0^o). Shown on the left side of the figure are contours of mixture fraction (dashed lines) and streamlines (solid lines). The mixture fraction, Z, is defined as

$$Z = \frac{1 + Y_F - Y_O}{2} \tag{22}$$

and the stoichiometric value is 0.5 under the assumption of equal molecular weight. The corresponding contours of reaction rates overlapped by the temperature contour lines are shown on the right hand side. The orientation of the figures is arranged with fluids entering into the bottom boundary and leaving from the top. As such, the top two figures represent a triple flame propagating toward the unburned fuel and oxidizer subject to a gravity force pointing downward referring to as the 'upright' flame. The middle figures are the computed results without gravity force. The bottom figures correspond to the

same flame but subject to a gravity force pointing upward referring to as the 'inverted' flame.

As defined earlier, the Froude number is positive when the gravity force is pointed downward in the same direction of the flame propagation, and vice versa. When the Froude number is positive, buoyancy causes acceleration of the flow above the triple flame tip as density decreases. The opposite effect occurs when the gravity force is reserved in direction. In comparison with the triple flame without gravity force, buoyancy results in a narrower triple flame when the gravity force is pointed downward. As the gravity force is reversed a wider triple flame is seen. Therefore, the flame shape is strongly affected by buoyancy and by the direction of the gravity vector. Moreover, due to buoyancy, the changes of the downstream flow field induce modifications of the mixing layer ahead of the triple flame via flow field divergence such that the propagating speed is altered.

Detailed profiles of the relevant variables along the stoichiometric line are presented in Figures 3 and 4. Figure 3 shows the effect of buoyancy on the stream-wise fluid velocity, displacement speed, and the propagating speed. As expected, buoyancy has a large impact on the fluids above the triple flame tip. The displacement speed is seen less sensitive to buoyancy. The propagation speed defined by Eq. (21) is flat over a region around the peak of displacement speed. Consequently, we simply take the maximum propagation speed evaluated along the stoichiometric line as the representative propagating speed. The propagation speed is reduced when the Froude number is positive which is consistent with recent experiments by Long et al. 1999. The corresponding profiles of mixture fraction gradient, temperature, and reaction rate are shown in Figure 4. Consistent with the qualitative flow pattern seen in Fig. 2, the mixture fraction gradient increases when the buoyancy accelerates the fluid above the triple flame tip. The opposite is seen when the Froude number is negative. The computed peak reaction rate and temperature at the triple flame tip are not affected by buoyancy. However, the reaction rate along the diffusion branch is seen to increase when the triple flame becomes narrower (cases with positive Froude numbers). This is due to increased diffusion of fuel and oxidizer as the flame gets narrower.

Relation between Propagation Speed and Buoyancy

A series of simulations have been conducted to explore the relation between the triple flame propagation speed and the two different Froude numbers defined in Eqs. (18) and (19). Cases, A, B, and C listed in Table 1 were conducted to reveal the dependence of propagation speed on the inlet mixing width of fuel and oxidizer as well as on gravity force. Since S_p decreases with the width of mixing layer, we plot the propagation speed normalized by its value at zero gravity versus $1/Fr_w$ in Fig. 5. As revealed in the figure, when the inlet mixture fraction gradient is increased by decreasing *W*, the flame propagating speed becomes more sensitive to buoyancy. The relation between $S_p / S_p(|\vec{g}=0|)$ and $1/Fr_w$ does not fall into a single curve. A simplified analysis of the buoyancy effect on S_p is described in the Appendix and the result suggests the following relation in the limit of small gravity force

$$\frac{S_p}{S_p(|\vec{g}=0|)} \approx \sqrt{1-C_0\frac{\rho_\infty}{\rho_0}\frac{1}{Fr_{L_f}}} \equiv \sqrt{1-X}\ , \tag{23}$$

where C_0 is a constant to be determined and $X \equiv C_0\frac{\rho_\infty}{\rho_0}\frac{1}{Fr_{L_f}}$. This correlation is limited to triple flames with small values of X. As the density ratio appears in Eq. (23), Case D listed in Table 1 is conducted with ρ_0/ρ_∞ being half of that in other cases in order to test the density ratio dependence. In addition, Cases E and F are conducted with different laminar flame speeds so that different sets of Fr_{L_f} can be used for assessing the validity of Eq. (23). Figure 6 presents a comparison of computed triple flame propagation speeds and the simplified model with C_0=10. The agreement is good except for large values of X where the assumption of small gravity force is not valid. Also indicated in the figure are estimated ranges of X under normal gravity for stoichiometric methane-air combustion and those with a fuel mixture of 77% N_2 and 23% H_2 by volume. The later has the same laminar flame speed as methane-air premixed flame but with a flame thickness about four times larger. These estimates are seen to fall into the regions where Eq. (23) is accurate. Consequently, Eq. (23) may be used as a semi-empirical correlation for estimating the effect of buoyancy on triple flames with practical fuels.

Effect of Orientation of Gravity on Triple Flames

Simulations were conducted to explore the effect of direction of gravity force on the orientation of triple flames. Figure 7 depicts the computed results in terms of contour plots of reaction rate overlapped by streamline. The magnitude of gravity was kept at Fr_w=1 and W=4L_f while the direction of gravity was changed. Simulations were conducted with ϕ varied from 0 to 180 degrees at every 45 degrees. According to Figure 5, the buoyancy effect at Fr_w=1 changes the triple flame propagation speed by about 25%. As seen in Figure 7 the orientation of triple flames responses to the direction of gravity force resulting in distortion of flame shape and upstream flow pattern.

CONCLUSIONS

The influence of buoyancy on the propagation speed and structure of triple flames in a two-dimensional scalar mixing layer is studied numerically with a wide range of parameters, including the mixing width, the amount of heat release, and the magnitude of gravity force. The numerical results revealed that buoyancy influences the fluid dynamics surrounding the triple flame causing changes in flame shape and propagation speed. When the gravity force is pointed in the direction of triple flame propagation, buoyancy causes acceleration of fluids downstream of the triple flame tip. In comparison to triple flames without buoyancy effects, the two premixed flame branches are brought closer to the diffusion branch leading to a less divergent flow pattern ahead of the triple flame. In response to the changes in fluid dynamics, the propagation speed of triple flame decreases and the fuel consumption rate of the diffusion branch increases. The opposite

trend is found for triple flames subject to gravity force pointed in the direction against the flame propagation. A simplified analytical model for the buoyancy effect on triple flame propagation speed is proposed for the limiting case of small gravity force. Comparisons the analytical model with the numerical results is reasonably good for a wide range of gravity, heat release, and mixing width.

ACKNOWLEDGMENTS

Support of this work is provided by NASA Lewis Center Microgravity Combustion Sciences Grant NAG3-2221 under the technical monitoring of Dr. Uday Hegde.

REFERENCES

Azzoni, R., Ratti, S., Agrawal, S.K., and Puri, I.K., *Combust. Flame*, 119:23-40 (1999).

Agrwal, A.K., Al-Ammar, K., Gollahali, S.R., and Griffin, D.W., *in the Proceedings of the Fifth International Microgravity Combustion Workshop*, NASA/CP report 1999-208917, 1999.

Buckmaster, J. and Matalon, M. 22nd *Symposium (Int.) on Combustion*, pp. 1527-1535, 1988.

Chen, J.Y. and Echekki, T., *"*Numerical Study of Buoyancy and Differential Diffusion Effects on the Structure and Dynamics of Triple Flames,*" in the Proceedings of the Fifth International Microgravity Combustion Workshop*, NASA/CP report 1999-208917, 1999, pp. 427-430.

Chung, S.H. and Lee, B.J. , *Combust. Flame*, 86:62-72. (1991).

Daou, J, and Linan, A, *Combustion Theory and Modeling*, 2:449-477 (1998).

Echekki, T. and Chen, J.H., *Combust. Flame*, 114:231-245 (1998).

Ghosal, S. and Vervisch, L., "Theoretical and Numerical Study of a Symmetrical Triple Flame Using the Parabolic Flame Path Approximation," Accepted by *J. Fluid Mechanics*, 2000.

Hartley, L.J. and Dold, J.W., *Combust. Sci. and Tech* 80:23-46 (1991).

Kioni, P.N., Rogg, B., Bray, N.C., and Linan, A., *Combust. Flame* 95:276-290 (1993).

Lee, B.J., Kim, J.S., and Chung, S.H., *25th Symposium (Int.) on Combustion*, pp. 1175-1181, 1994.

Lee B.J. and Chung S.H., *Combust. Flame*, 109:163-172 (1997).

Long, M.B., Walsh. K.T., and Smooke, M.D., "The Effects of Buoyancy and Dilution on the Structure and Lief-Off of Coflow Laminar Diffusion Flames," *in the Proceedings of the Fifth International Microgravity Combustion Workshop*, NASA/CP report 1999-208917, 1999, pp. 105-110.

Poinsot, T and Lele, S., *J. Computational Physics*, 101:104-129 (1992).

Phillips, H., *10th Symposium (Int.) on Combustion*, pp.1227-1283, 1965.

Ruetsch, G.R., Vervisch, L. and Linan, *A., Phys. Fluids*, 7(6):1447-1454 (1995).

Ruetsch, G.R. and Ferziger, J.H., *Center for Turbulence Research NASA Ames/Stanford University, Annual Research Briefs*, 1996, pp. 67--84.

Domingo, P., and Vervisch, L., *26th Symposium (Int.) on Combustion*, pp.233, 1996.

Plessing, T., Terhoeven, P., Peters, N., and Mansour, M.S., *Combust. Flame* 115:335-353 (1998).

Vedarjan, T.G., and Buckmaster, J., *Combust, Flame* 114:267-273 (1998).

Table 1 Simulation conditions and the range of gravity force[1].

Case	α	W / L_f	$S_L / S_L(A)$ [2]	ρ_0 / ρ_∞ [3]	$1/Fr_w$ [4]	$1/Fr_{L_f}$ [4]
A	0.85	2	1	6.67	(-2.0 → 1.0)	(-1.0 →0.5)
B	0.85	4	1	6.67	(-2.0 →2.0)	(-0.5 →0.5)
C	0.85	8	1	6.67	(-8.0 →5.0)	(-1.0 →0.625)
D	0.70	4	1	3.34	(-4.0 →2.0)	(-1.0→0.5)
E	0.85	3.2	0.8	6.67	(-3.0 →1.75)	(-0.938 →0.547)
F	0.85	4.8	1.2	6.67	(-2.0 →1.75)	(-0.417→0.365)

[1]Under all conditions, β=8, $\rho_0 \Lambda L_f / S_L$ =11,340, $\mathrm{Re}_0 (= S_L L_f / \nu_0)$ =5.64.

[2] $S_L / S_L(A)$ denotes the ratio of planar premixed flame speed of stoichiometric mixture and that under conditions of Case A.

[3] ρ_∞ is the density of completely burned stoichiometric mixture.

[4]($a \rightarrow b$): *a* denotes the lower limit and *b* the upper limit. Positive values correspond to triple flames propagating downward with gravity pointed downward ($\phi=180^o$). Negative values correspond to triple flames propagating downward with gravity pointed upward ($\phi=0^o$).

Appendix Simplified Analysis of Buoyancy Effects on Triple Flames

Following Ruetsch, et al., (1995), Figure 8 depicts the geometry of a triple flame subject to a gravity force pointed downward. We have used g to represent the magnitude of gravity vector. Using the Rankine-Hugoniot relation across the points 2 and 3, we have

$$\rho_2 u_2 = \rho_3 u_3 \tag{A1}$$

$$p_2 + \rho_2 u_2 = p_3 + \rho_3 u_3 . \tag{A2}$$

Along the streamline at the center, Bernoulli's equations give the following results for segments from point 1 to point 2 and from point 3 to point 4

$$p_1 + \frac{1}{2}\rho_1 u_1^2 + \rho_1 g x_1 = p_2 + \frac{1}{2}\rho_2 u_2^2 + \rho_2 g x_2 \tag{A3}$$

$$p_3 + \frac{1}{2}\rho_3 u_3^2 + \rho_3 g x_3 = p_4 + \frac{1}{2}\rho_4 u_4^2 + \rho_4 g x_4 \tag{A4}$$

Let's denote $L_1=x_2-x_1$ and $L_2=x_4-x_3$, and assume that $\rho_1=\rho_2$, $\rho_3=\rho_4$, and $\rho_1 u_1 \delta_1 \approx \rho_4 u_4 \delta_4$. With these assumptions, we can combine Eqs. (A1)-(A4) leading to the following result

$$\left(\frac{u_1}{u_2}\right)^2 = \frac{\dfrac{\rho_1}{\rho_4}-1}{\dfrac{p_1 - p_4 - (\rho_1 L_1 + \rho_4 L_2)g}{\frac{1}{2}\rho_1 u_1^2} - \dfrac{\rho_1}{\rho_4}\left(\dfrac{\delta_1}{\delta_4}\right)^2 + 1}. \tag{A5}$$

The difference between the background hydrostatic pressures without combustion at point 4 and point 1 is $p_{s,1} - p_{s,4} = \rho_1 (L_1 + L_2) g$. Expressing the pressure as $p=p_s+p'$, we can rewrite Eq. (A5) as

$$\left(\frac{u_1}{u_2}\right)^2 = \frac{\dfrac{\rho_1}{\rho_4}-1}{\dfrac{p'_1 - p'_4 + (\rho_1 - \rho_4) L_2 g}{\frac{1}{2}\rho_1 u_1^2} - \dfrac{\rho_1}{\rho_4}\left(\dfrac{\delta_1}{\delta_4}\right)^2 + 1} \tag{A6}$$

Ruetsch, et al., (1995) assumed $p'_1 \approx p'_4$ and $u_1 \approx u_4$ for triple flames without buoyancy effects. In the limit of small gravity force, these assumptions are applicable and the following result emerges

$$\left(\frac{u_1}{u_2}\right)^2 = \frac{\dfrac{\rho_1}{\rho_4}-1}{\dfrac{(\rho_1 - \rho_4) 2 L_2 g}{\rho_1 u_1^2} - \dfrac{\rho_4}{\rho_1} + 1} = \frac{\rho_1}{\rho_4}\frac{1}{\dfrac{2 L_2 g}{u_2^2}\left(\dfrac{u_2^2}{u_1^2}\right) + 1}. \tag{A7}$$

Solving for u_1/u_2, we obtain

$$\frac{u_1}{\sqrt{\dfrac{\rho_1}{\rho_4}} u_2} = \sqrt{1 - \frac{\rho_4}{\rho_1}\frac{2 L_2 g}{u_2^2}} . \tag{A8}$$

For triple flames without gravity force (g=0), Eq. (A8) reduces to $u_1 = \sqrt{\rho_1/\rho_4}\,u_2$ which is identical to that from the analysis by Ruetsch, et al., (1995). Note that $u_1=S_p$ and $u_2=S_L$, we have $S_p(g=0) = \sqrt{\rho_1/\rho_4}\,S_L$ which provides an estimate of the effect of flow divergence on propagation speed. We can rewrite Eq. (A8) using the notations in the main text ($\rho_1=\rho_0$ and $\rho_4=\rho_\infty$) as

$$\frac{S_p}{S_p(g=0)} = \sqrt{1-\frac{\rho_\infty}{\rho_0}\frac{2L_2 g}{S_L^2}} \tag{A9}$$

with L_2 being the size of region where buoyancy effect is most influential to the divergence of the flow field. As the curvature of triple flame decreases with increasing mixing width, W, we anticipate L_2 decrease with increasing W. If we assume that L_2/δ_1 scales with L_f/W, Eq. (A9) becomes

$$\frac{S_p}{S_p(g=0)} \approx \sqrt{1-C\frac{\rho_\infty}{\rho_0}\frac{\delta_1}{W}\frac{L_f g}{S_L^2}} \approx \sqrt{1-C_0\frac{\rho_\infty}{\rho_0}\frac{1}{Fr_{L_f}}}\,, \tag{A10}$$

where C_0 is a constant to be determined. In the above derivation, the ratio, δ_1/W, is assumed constant. As δ_1 is the width of inlet streams encompassing the triple flame, it is expected to scale linearly with the mixing width, W.

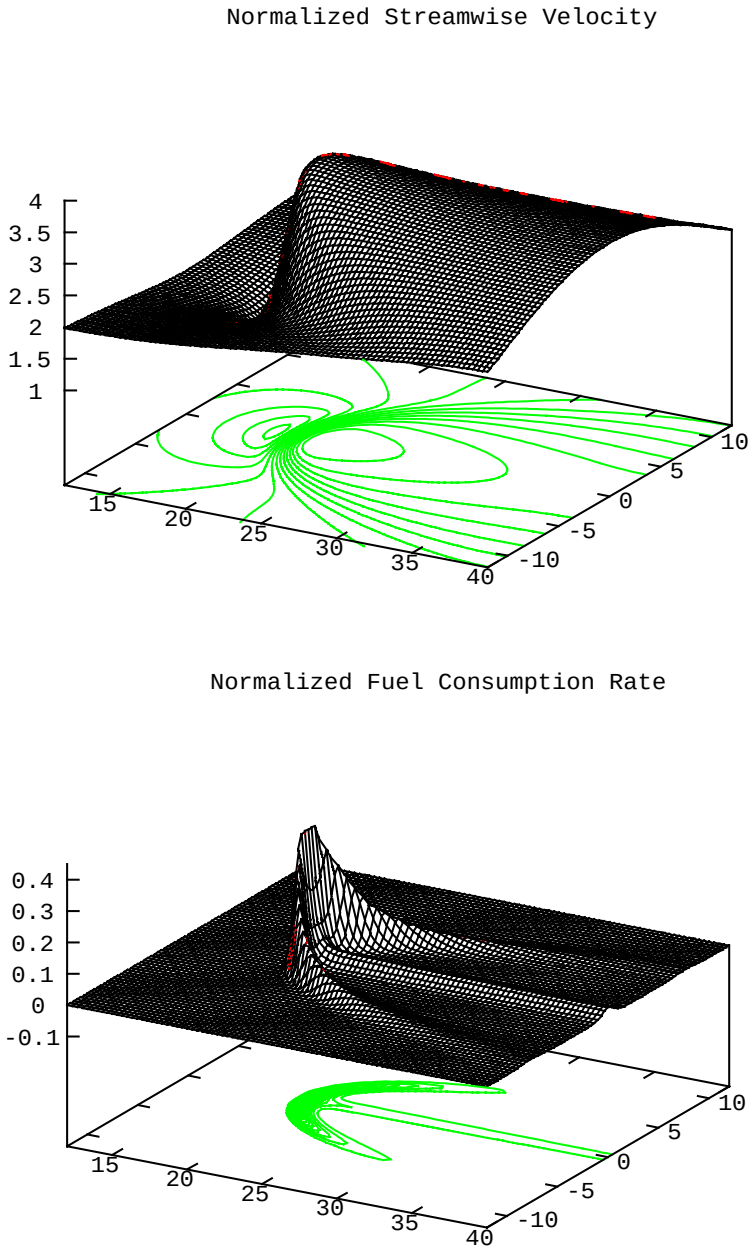

Fig. 1 Characteristics of triple flames obtained with a two-dimensional simulation with inlet flow coming from the left and leaving to the right. A mixing layer of fuel and oxidizer is imposed on the inlet. Lengths are units of premixed flame thickness. Top: stream-wise velocity normalized by premixed stoichiometric flame speed. Bottom: fuel consumption rate.

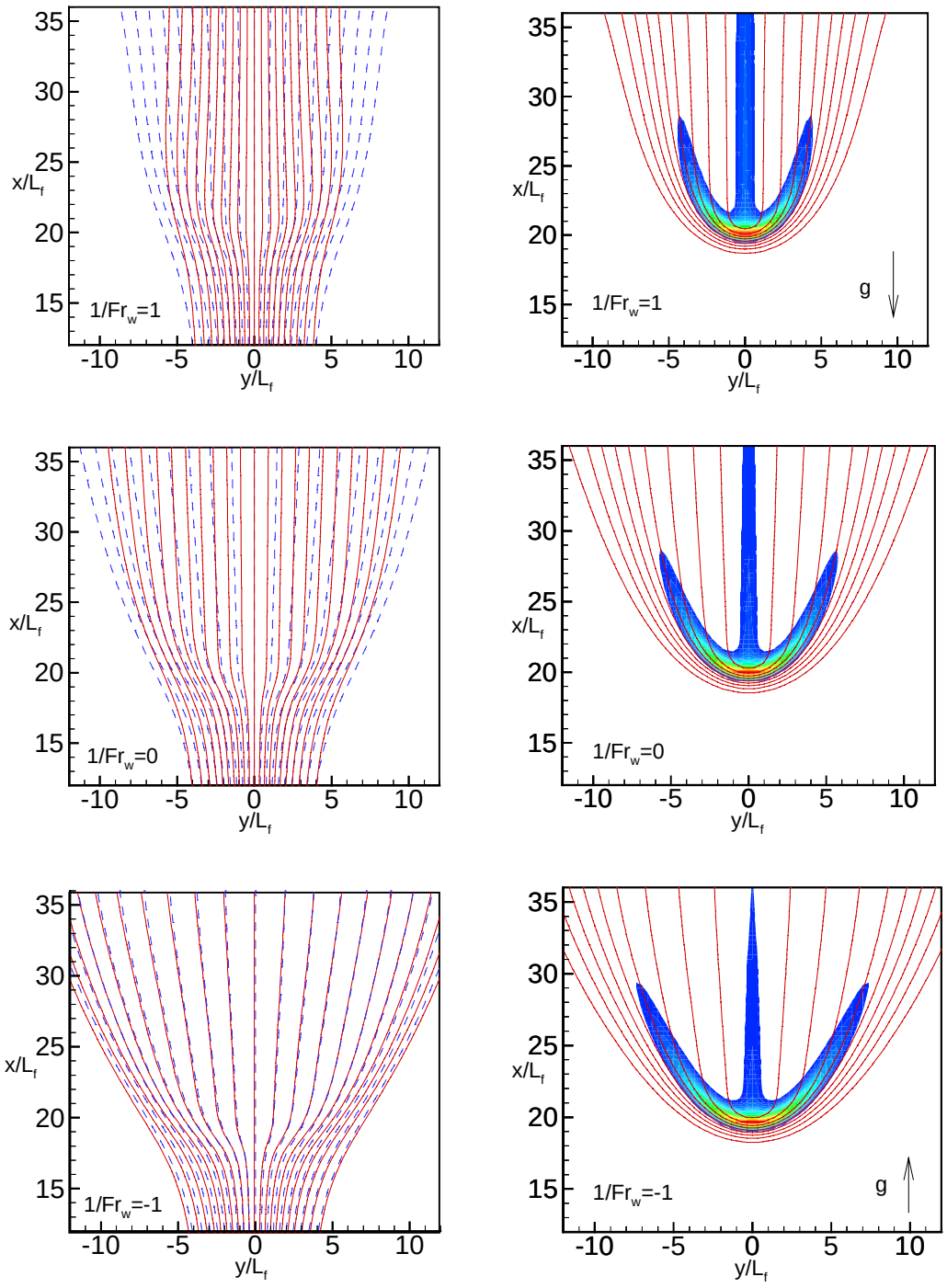

Fig. 2 Effects on buoyancy of triple flames in views of streamlines (solid lines) and constant mixture fraction contours (dashed lines) on left and reaction rate overlapped by constant temperature contours (lines) on right. Top: with gravity force pointed downward in the same direction of triple flame propagation; middle: without gravity force; bottom: with gravity force pointed upward in the opposite direction of triple flame propagation. Lengths are units of premixed flame thickness.

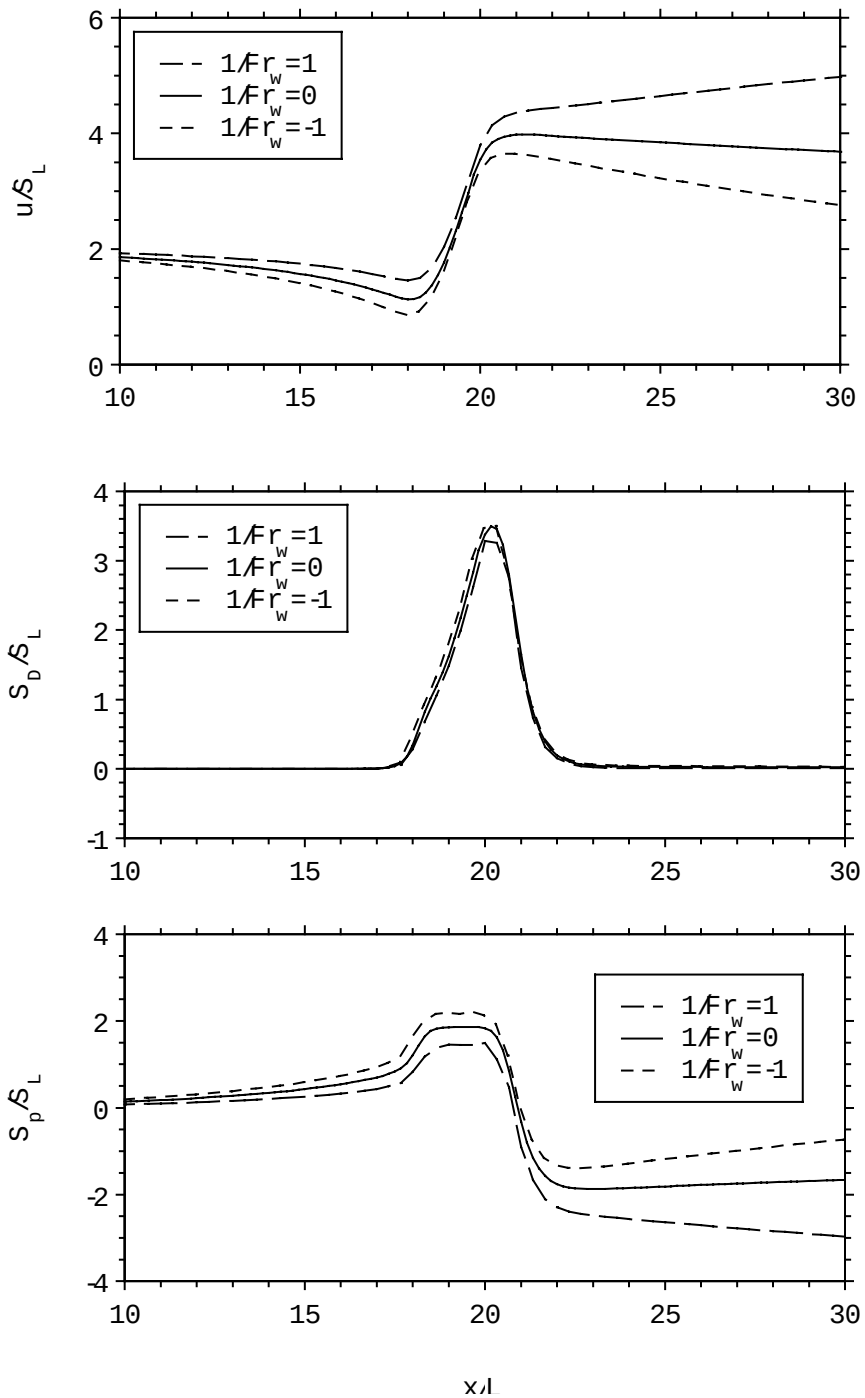

Fig. 3 Influences of buoyancy on characteristic velocities along the stoichiometric line y=0). Simulations were conducted without gravity force ($1/Fr_W=0$) and with gravity forces pointed downward ($1/Fr_W=1$, $\phi=180^o$) and upward ($1/Fr_W=-1$, $\phi=0^o$). Top: stream-wise velocity; middle: displacement speed; bottom: propagation speed. All speeds are normalized by planar premixed stoichiometric flame speed.

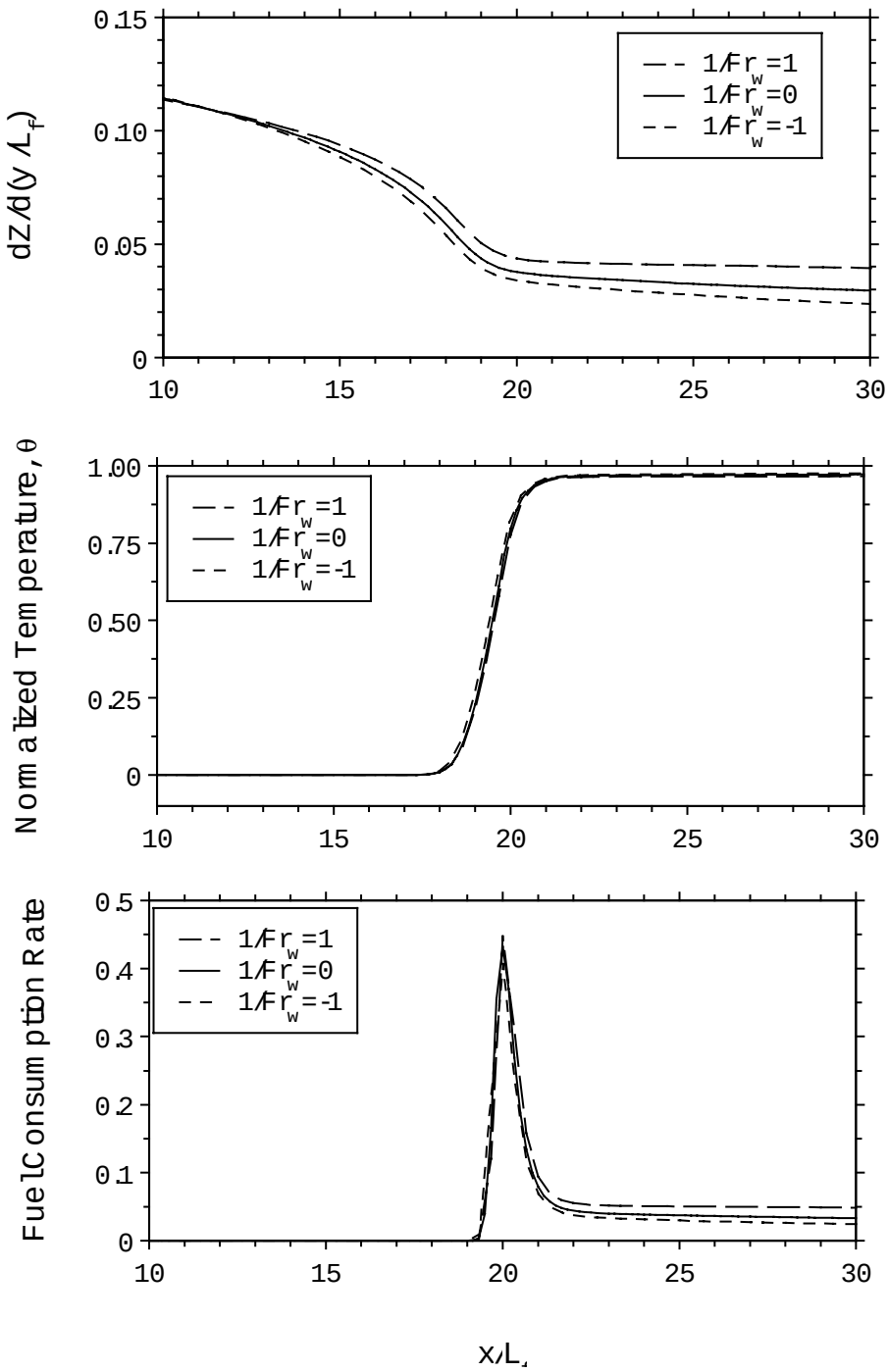

Fig. 4 Effects of buoyancy on triple flame structures along the stoichiometric line (y=0, Z=0.5). Simulations with gravity forces pointed downward ($1/Fr_W$=1, ϕ=180^o) and upward ($1/Fr_W$=-1, ϕ=0^o). Reference case without gravity force ($1/Fr_W$=0). Top: normalized mixture fraction gradient in the transverse flow direction; middle: normalized temperature; bottom: normalized fuel consumption rate.

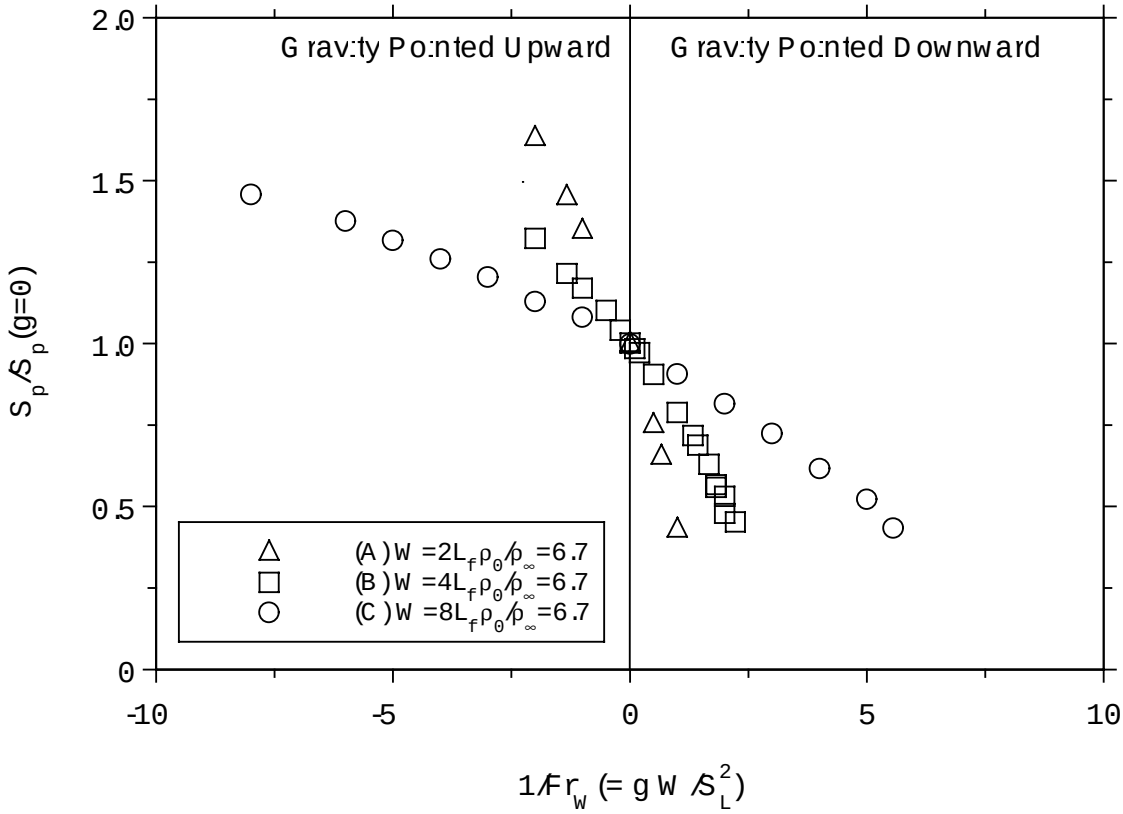

Fig. 5 Computed correlation between triple flame propagation speed normalized by its value at zero gravity and the Froude number based on inlet mixing width of fuel and oxidizer at inlet. The triple flames propagate downward and the gravity forces are either pointed upward or downward. Details of conditions are listed in Table 1. The relations are seen to depend on the width of mixing layer and there is no simple relation exists.

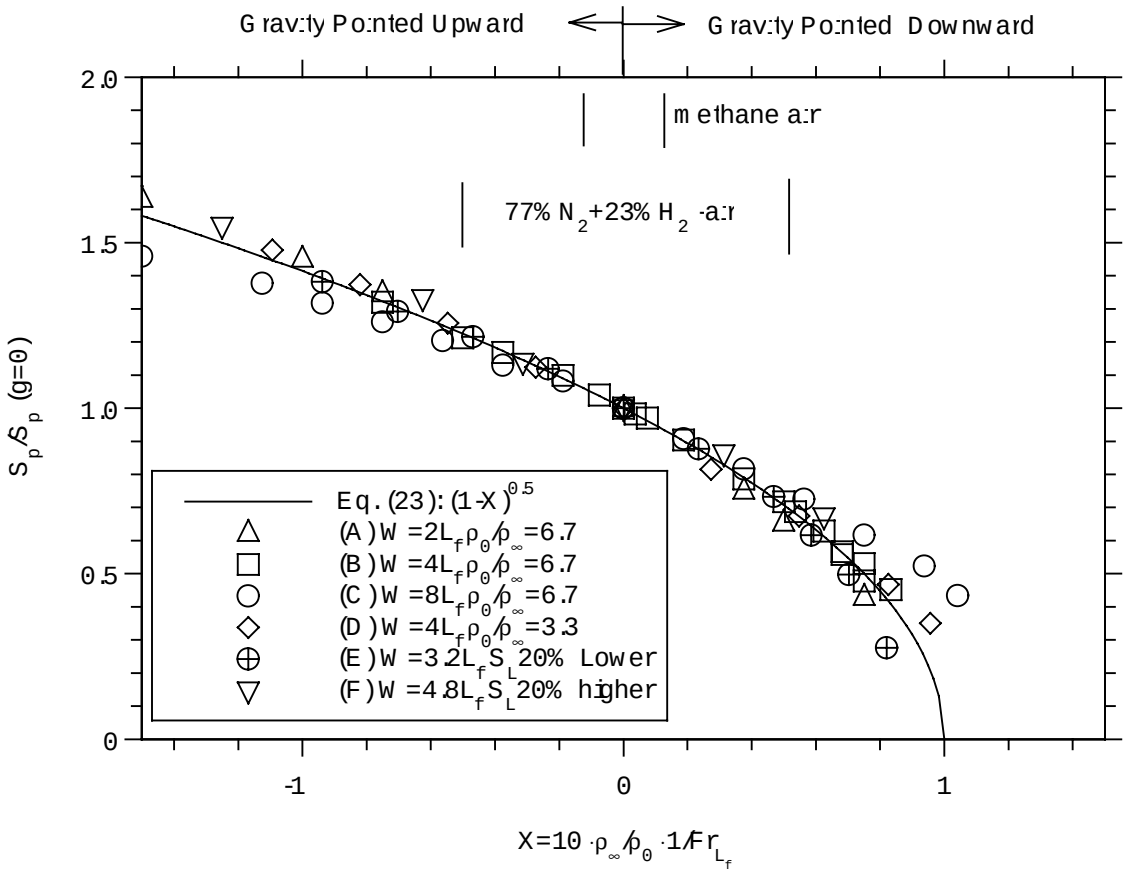

Fig. 6 Computed correlation between triple flame propagation speed normalized by its value at zero gravity and the Froude number based on the thickness of planar premixed stoichiometric flame. The triple flames propagate downward and the gravity forces are either pointed upward or downward. Details of conditions are listed in Table 1. The relations are seen to collapse onto one curve closely represented by Eq. (23).

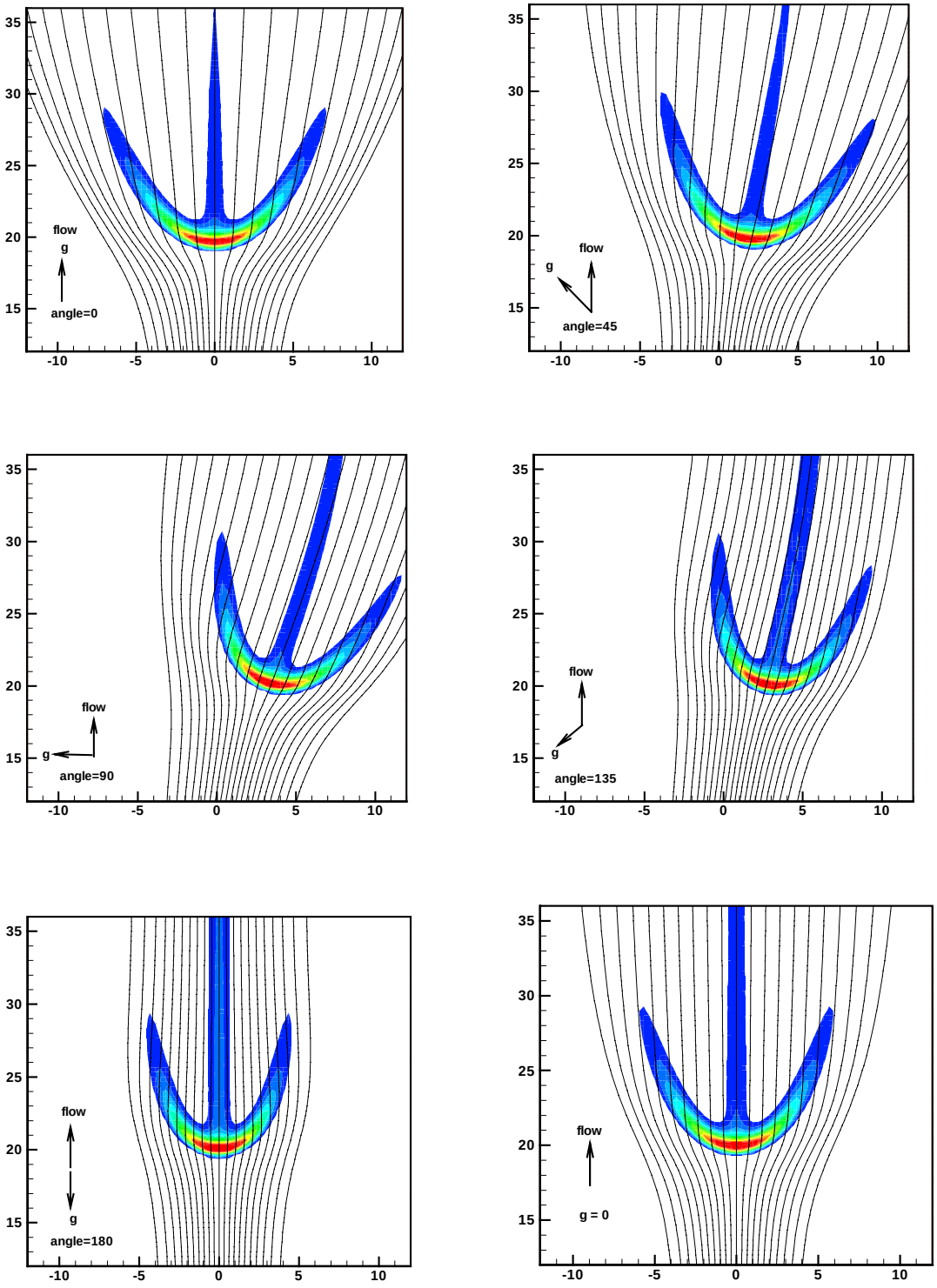

Fig 7 Effect of orientation of gravity on triple flames plotted as reaction rate contours overlapped by streamlines. The magnitude of gravity force is fixed while the orientation of gravity forces is varied every 45 degrees showing a strong impact of gravity on the shape. Lengths are units of flame thickness.

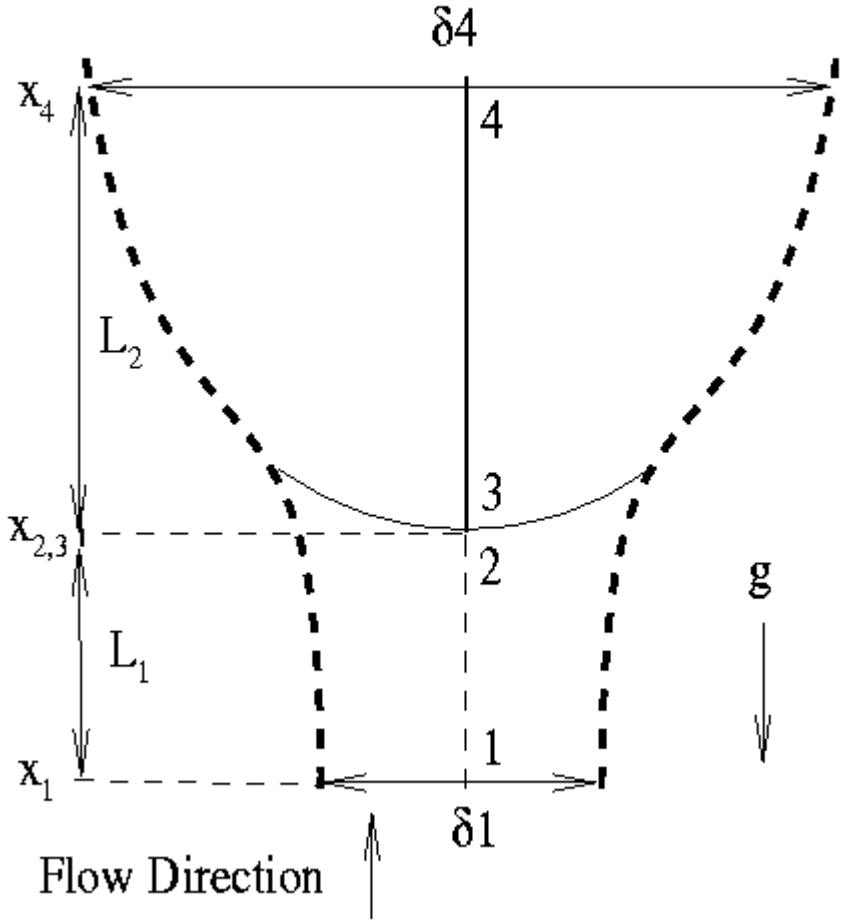

Fig. 8 Schematic of a triple flame subject to gravity force pointed downward in the same direction as the triple flame propagation. Heavy dashed lines: streamlines enclosing the triple flame; thick solid lines: triple flames anchored at point 2 with segment 3-4 denoting the trailing diffusion flame branch and the arc representing the two premixed flame branches. Distance L_2 is the size of region most affected by buoyancy force due to density changes.δ_1 and δ_4 are the sizes of stream tube at point 1 and 4 respectively.